Heliyon 9 (2023) e21765

Contents lists available at ScienceDirect

Heliyon

journal homepage: www.cell.com/heliyon

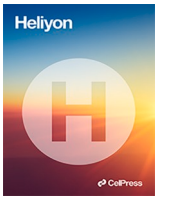

Lithium aluminum hydride Li_3AlH_6: new insight into the anode material for liquid-state lithium-ion batteries

Chu Liang [a,c,*], Zhangze Ye [a], Yaxiong Yang [b], Huilong Jing [a], Haihuang Wu [a], Yanxia Liu [b], Xiaoyu Zhang [a,**], Zhihe Liu [d], Hongge Pan [a,b,c]

[a] Zhejiang Carbon Neutral Innovation Institute & Moganshan Institute of ZJUT at Deqing, Zhejiang University of Technology, Hangzhou 310014, China
[b] Institute of Science and Technology for New Energy Xi'an Technological University Xi'an 710021, China
[c] School of Materials Science and Engineering, Zhejiang University, Hangzhou 310027, China
[d] Department of Chemical and Biomolecular Engineering National University of Singapore 4 Engineering Drive 4, Singapore 117585, Singapore

A B S T R A C T

Metal hydrides have been demonstrated as one of the promising high-capacity anode materials for Li-ion batteries. Herein, we report the electrochemical properties and lithium storage mechanism of a Li-rich complex metal hydride (Li_3AlH_6). Li_3AlH_6 exhibits a lithiation capacity of ~1729 mAh/g with a plateau potential of ~0.33 V vs. Li^+/Li at the first discharge cycle. Experimental results demonstrate that Li_3AlH_6 is converted into LiH and LiAl in the initial electrochemical lithiation process. In addition, Li_3AlH_6 also possesses a good cycling stability that 71 % of the second discharge capacity is retained after 20 cycles. More importantly, the cycling performance of Li_3AlH_6 can be improved to 100 cycles via adjusting electrolyte composition. This study provides a new approach for developing the lithium storage properties of anode materials for Li-ion batteries.

1. Introduction

Li-ion battery has now been widely used as portable power sources in electronic devices such as laptop computers, cellular phones, intercoms, digital cameras, music players, and so on [1,2]. It is also regarded as one of the promising batteries for power electric vehicles and large machines. Currently, graphite has been widely applied as the major anode materials in the commercial Li-ion batteries due to its low cost, satisfying cycle life, and low working potential [3,4]. Unfortunately, graphite anodes suffer from a specific capacity limitation (372 mAh/g), which leads to a large obstacle to developing high-capacity lithium-ion batteries for the future market demand [5]. Alloying reaction and conversion reaction anodes have been demonstrated as effective strategies to obtain higher specific capacity [6]. A series of new materials, such as lithium alloys [7–12], metal oxides [13–16], sulphides [17–19], nitrides [20,21], and so on, have been widely explored as high-capacity anode candidates for Li-ion batteries. As a typical example, silicon could possess a high theoretical capacity of 3590 mAh/g via alloying reaction [22]. However, its huge volume expansion/contraction in the electrochemical alloying/dealloying process severely hinders its practical application [23]. Ferric oxide could exhibit a theoretical capacity of 1007 mAh/g through a conversion reaction. High working potential and large potential hysteresis for ferric oxide anodes are still the considerable disadvantages [24]. Therefore, searching for anode materials with high capacity and low working

* Corresponding author. Zhejiang Carbon Neutral Innovation Institute & Moganshan Institute of ZJUT at Deqing, Zhejiang University of Technology, Hangzhou 310014, China.
** Corresponding author. Zhejiang Carbon Neutral Innovation Institute & Moganshan Institute at Deqing, Zhejiang University of Technology, Hangzhou 310014, China.
E-mail addresses: cliang@zjut.edu.cn (C. Liang), zhangxiaoyu@zjut.edu.cn (X. Zhang).

https://doi.org/10.1016/j.heliyon.2023.e21765
Received 17 July 2023; Received in revised form 28 September 2023; Accepted 27 October 2023
Available online 2 November 2023
2405-8440/© 2023 The Authors. Published by Elsevier Ltd. This is an open access article under the CC BY-NC-ND license (http://creativecommons.org/licenses/by-nc-nd/4.0/).

potential is crucial for the further practical Li-ion batteries with high energy density.

Metal hydrides and metal hydroxides have been regarded as ideal potential candidates to high-capacity anode materials toward Li-ion batteries [25,26]. For instance, Gao et al. [27] reported that the space-confined MgH_2 and Mg_2NiH_4 could exhibit a large reversible capacity (1392 mAh/g) with an average plateau potential of ~0.5 V vs. Li^+/Li through the conversion reactions ($MgH_2+2Li+2e^-\rightarrow Mg+2LiH$, $Mg_2NiH_4+4Li+2e^-\rightarrow Mg_2Ni+4LiH$). Luo et al. [28] reported dodecyl sulfate anions intercalated nickel-zinc layered double hydroxide (NZDS) which exhibits high capacity of 850 mAh g^{-1} at 0.5 A g^{-1} for long cycles. Li-rich complex metal hydrides have been extensively investigated as high-capacity hydrogen storage materials [29,30]. Mo et al. reported three-dimensional hierarchical $LiNa_2AlH_6$/graphene composites ($LiNa_2AlH_6$/3DG) with a high initial discharge capacities of 2396 mA h/g [31]. Therefore, it might be an effective strategy to design Li-rich complex metal hydrides as anode materials towards Li-ion batteries.

In this work, we synthesized a Li-rich complex metal hydride (Li_3AlH_6) via ball milling by $LiAlH_4$ with LiH. The synthesized Li_3AlH_6 as the anode material for Li-ion batteries exhibits a lithiation capacity of ~1729 mAh/g with a plateau potential of ~0.33 V vs. Li^+/Li at the first discharge cycle. In addition, Li_3AlH_6 possesses a high cycling stability with 71 % of second discharge capacity after 20 cycles. Experimental results demonstrate that the electrochemical lithium storage in Li_3AlH_6 can be described as $Li_3AlH_6+4Li^++4e^-\rightarrow 6LiH + LiAl\leftrightarrow 6LiH + Al+Li^++e^-$. That is, Li_3AlH_6 is converted into LiH and LiAl in the first electrochemical lithiation process, while LiH and LiAl could not reverted to the initial electrode material of Li_3AlH_6.

2. Resultes and discussion

The synthesis procedure of Li-rich complex metal hydride, Li_3AlH_6, via ball milling by $LiAlH_4$ with LiH is illustrated in Fig. 1a (see Experimental Section for details). During the 24 h high-energy ball milling process, ~0.44 wt% of hydrogen was released. According to the synthesis equation, it is calculated that 0.44 wt% of hydrogen corresponds to ~7 % of Li_3AlH_6, a ~93 % purity of Li_3AlH_6 was obtained. This purity is consistent with the result concluded from dehydrogenation of Li_3AlH_6 (Fig. S1c). Subsequently, the electrode material was prepared via low-energy ball milling of Li_3AlH_6 and acetylene black with a weight ratio of 85:15. The electrode material was demonstrated to be the mixture of Li_3AlH_6 and acetylene black, determined via X-ray diffraction (XRD) pattern, Fourier Transform Infrared Spectrometer (FTIR), and Raman spectra (Fig. S1). The electrochemical lithium storage properties of Li_3AlH_6 were evaluated by galvanostatic discharge-charge measurements. Fig. 1b and c show the discharge and charge potential profiles of the Li_3AlH_6 electrode at a current density of 100 mA/g between 0.005 and 3.0 V vs. Li^+/Li, respectively. As shown in Fig. 1b, Li_3AlH_6 delivers a specific capacity of ~1729 mAh/g during the first discharge cycle, corresponding to about 3.5 mol Li. In addition, the potential drops to a long discharge plateau located at ~0.33 V and subsequently appears a slow decay before a short discharge plateau (~0.14 V). The plateau potential of Li_3AlH_6 is similar to that of metallic Al electrode (Fig. S2). In Fig. 1c, a plateau potential located at ~0.44 V and two sloping potential are observed during the first charging process. Unfortunately, only ~509 mAh/g that is equivalent to 1.0 mol Li is recharged in the first charging process. The initial coulombic efficiency of Li_3AlH_6 is only *ca.* 29.4 %, indicating that the Li_3AlH_6 after fully discharged could not reverted to its initial state completely under the present conditions.

To reveal the lithium storage mechanism, XRD measurements were conducted on Li_3AlH_6 samples from different lithium storage stages. Fig. 2a and b presents the XRD patterns of as-prepared Li_3AlH_6 discharged and recharged to the potential levels in Fig. 1b and c,

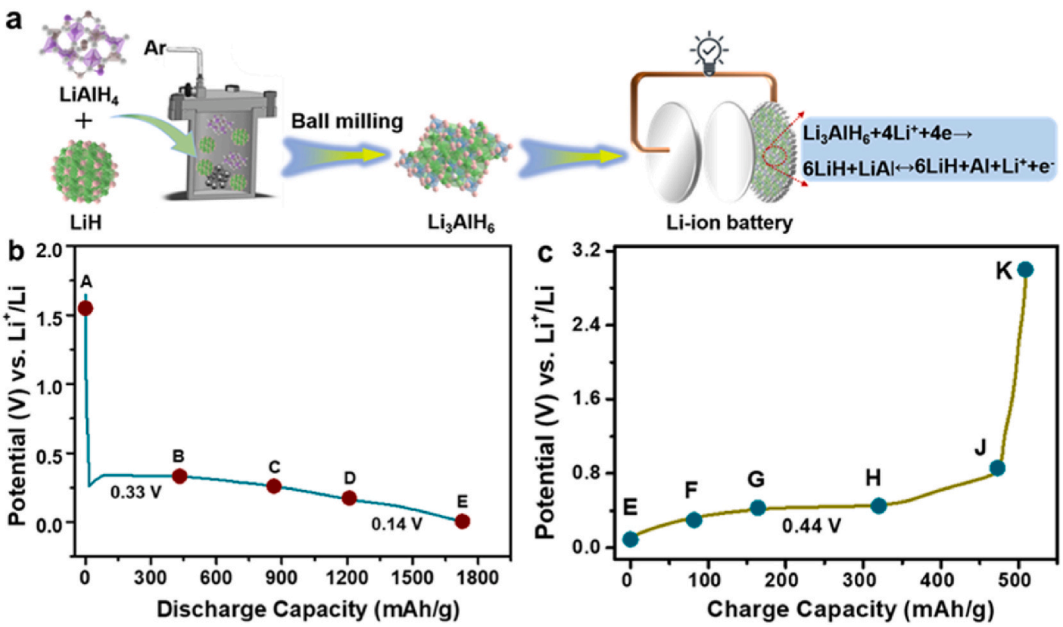

Fig. 1. (a) Schematic illustration of the synthesis of Li_3AlH_6. First-cycle discharge (b) and charge (c) potential profiles of as-prepared Li_3AlH_6.

respectively. In Fig. 2a, Li_3AlH_6 acts as the dominant phase (point A). Different from as-prepared Li_3AlH_6 (Fig. S1), the intensity of diffraction peak at 22.3° is obviously higher than that at 21.8° due to a side reaction of Li_3AlH_6 with electrolytes. At the stages of B and C point, LiH and metallic Al are both detected corresponding to the gradual disappear of Li_3AlH_6. After discharge to point D, LiAl as a new phase is identified, while Li_3AlH_6 is almost undetectable. When discharging to point E, the fully lithiated products are composed of LiAl and LiH. It is worth noting that the diffraction peaks located at 22.5, 25.5, and 26.7° are close to that of $Al_{13}Fe_4$ at 22.4, 25.1, and 26.6° [32], and then disappears with the consumption of metallic Al. The similar phenomenon is also observed in the following recharge process (Fig. 2b). This indicates that Al–Fe intermetallic might generate due to the reaction between a small amount of Fe with the material during the high-energy ball milling for the preparation of the Li_3AlH_6. Besides, another unknown phases with diffraction peaks at 12.1, 15.6, 17.8, 20.5, 22.3, and 23.8° are detected in the discharge process and appear in the recharge process, which may originate from the byproduct between the reaction of Li_3AlH_6 and electrolytes. To ascertain our speculation, the samples from different lithium storage stages were further examined by FTIR to testify the unknown phases that Li_3AlH_6 reacting with electrolytes (Fig. S3). The absorption peaks centered at 1807, 1778, 1406, 1324, 1199, and 1081 cm^{-1} correspond to the stretching vibrations of C═O, C–C, C–H, and C–F bonds, which are observed in the whole discharge and recharge process. Therefore, it can be known that the unknown phases are the product of Li_3AlH_6 reacting with electrolytes.

The Li_3AlH_6 electrode material was subjected to recharging after discharging to point E. As shown in Fig. 2, the intensity of LiAl diffraction peaks became weak with the recharge from E to G, until disappear at point H. While the intensity of diffraction peak at ~38.2°, corresponding to LiH and Al, gradually increases from E to H. Although the diffraction peaks of LiH located at 38.2, 44.4, 64.6, 77.6, and 81.8° are very close to those of Al (38.4, 44.7, 65.1, 78.2, and 82.4°), their relative intensities are quite distinct. This indicates that the LiAl is converted to metallic Al and Li during the recharge process. When the electrode further recharged to point J and K, the diffraction patterns almost unchanged. LiH and metallic Al are the major phases among the fully delithiated products, which indicates that the LiH and LiAl as lithiated products could not revert to the initial electrode material of Li_3AlH_6. Base on the above results, the electrochemical lithium storage in Li_3AlH_6 can be described as follows:

$$Li_3AlH_6 + 4Li^+ + 4e^- \rightarrow 6LiH + LiAl \leftrightarrow 6LiH + Al + Li^+ + e^-$$

According to this lithium storage reaction, Li_3AlH_6 exhibits an electrochemical capacity of ~1990 mAh/g, which is close to the experimental value (1729 mAh/g).

The electrochemical properties of the Li_3AlH_6 are evaluated as an anode material for Li-ion batteries. The electrochemical lithium storage behavior of the Li_3AlH_6 is first studied by cyclic voltammetry (CV). The representative CV curves of the first three cycles of the electrode in a voltage window of 0.005–3.0 V (vs. Li/Li^+) was presented in Fig. 3a. In the first cathodic scan, the irreversible electrochemical reduction reactions between Li_3AlH_6 and Li^+ occurs accompanying the formation of LiH and LiAl ($Li_3AlH_6 + 4Li^+ + 4e^- \rightarrow 6LiH + LiAl$). An obvious anodic peak at about 0.58 V can be assigned to the Li^+ extraction reaction. It is noteworthy that compared with the first cycle, the main cathodic peaks shift to ~0.33 V in the subsequent two cycles, while the anodic peaks show negligible change. This phenomenon further confirms the above electrochemical lithium storage in Li_3AlH_6 ($Li_3AlH_6 + 4Li^+ + 4e^- \rightarrow 6LiH + LiAl \leftrightarrow 6LiH + Al + Li^+ + e^-$), which corresponds to the XRD result. The stability performance is another prominent concern for an advanced anode material in Li-ion batteries. Fig. 3b illustrates the charge capacity of as-prepared Li_3AlH_6 as a function of cycle number. The discharge capacity of Li_3AlH_6 decreased dramatically from 1729 mAh/g at the first cycle to 509 mAh/g at the second cycle due to the partial reversibility of lithium storage in Li_3AlH_6. Fortunately, the as-prepared Li_3AlH_6 exhibits an approving cycling stability after the second cycle. The slight decay in the discharge capacity with 362 mAh/g after 20 cycles, realizing 71 % capacity retention relative to the second cycle. Compared with the bulk Al electrode with only 30 % capacity retention after 10 cycles [33], the Li_3AlH_6 electrode possesses an outstanding stability. Therefore, LiH that formed in the initial stage of the lithiation of Li_3AlH_6 acts as an inactive material, however, it as a volumetric expansion buffer plays an important role in relieving volume

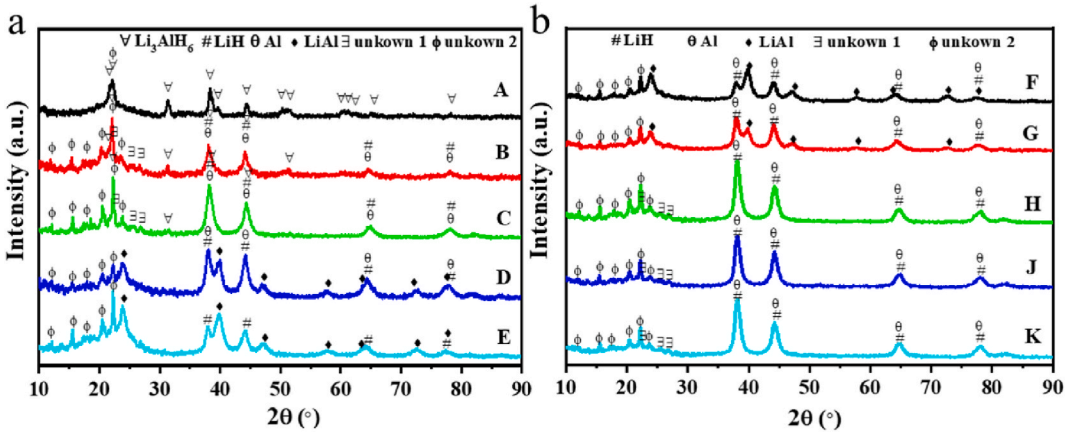

Fig. 2. XRD patterns of Li_3AlH_6 electrode material collected at various discharge (a) and recharge (b) stages. Capital letters denote the sampling points of the discharge and recharge experiment as shown in Fig. 1.

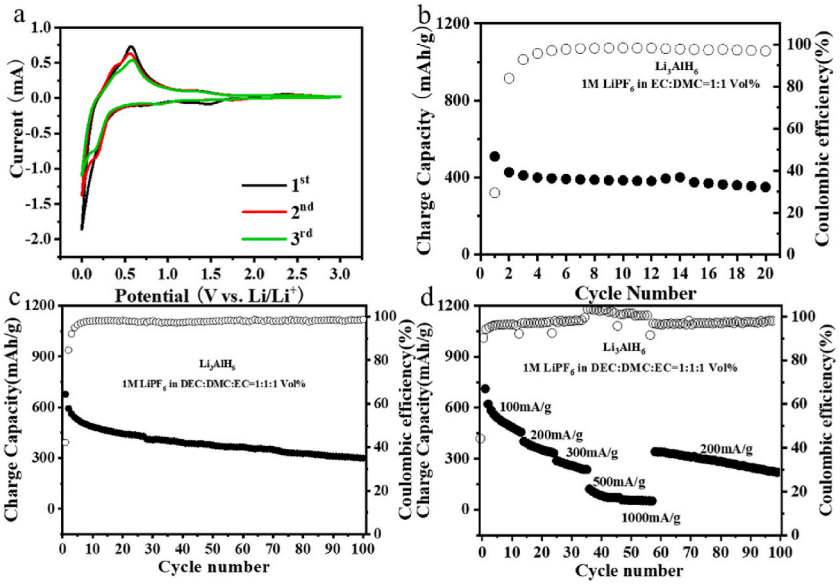

Fig. 3. (a) CV curves of Li_3AlH_6 in the voltage range of 0.005–3.0 V (vs. Li/Li^+) in electrolyte composed of 1 M $LiPF_6$ solution of ethylene carbonate and dimethyl carbonate with a weight ratio of 1:1. (b) Charge capacity of as-prepared Li_3AlH_6 as a function of cycle number. The cycle performances are cycled between 0.005 and 3.0 V (vs. Li^+/Li) at a current density of 100 mA/g in electrolyte composed of 1 M $LiPF_6$ solution of ethylene carbonate and dimethyl carbonate with a weight ratio of 1:1. (c) Charge capacity of as-prepared Li_3AlH_6 as a function of cycle number. The cycle performances are cycled between 0.005 and 3.0 V (vs. Li^+/Li) at a current density of 100 mA/g in electrolyte composed of 1 M $LiPF_6$ solution of ethylene carbonate, dimethyl carbonate, and diethyl carbonate with a weight ratio of 1:1:1. (d) Rate performance of as-prepared Li_3AlH_6. The cycle performances are cycled between 0.005 and 3.0 V (vs. Li^+/Li) in electrolyte composed of 1 M $LiPF_6$ solution of ethylene carbonate, dimethyl carbonate, and diethyl carbonate with a weight ratio of 1:1:1.

expansion in delithiation/lithiation process. On the other hand, the unknown phases from the partial reaction of Li_3AlH_6 with electrolytes may play a similar role with the solid electrolyte interface (SEI) layer.

Moreover, we found that the electrochemical lithium storage properties can be improved by adjusting the electrolyte composition. As shown in Fig. 3c, the cycling performance of Li_3AlH_6 increased from 20 cycles to 100 cycles in the new electrolyte that composed of

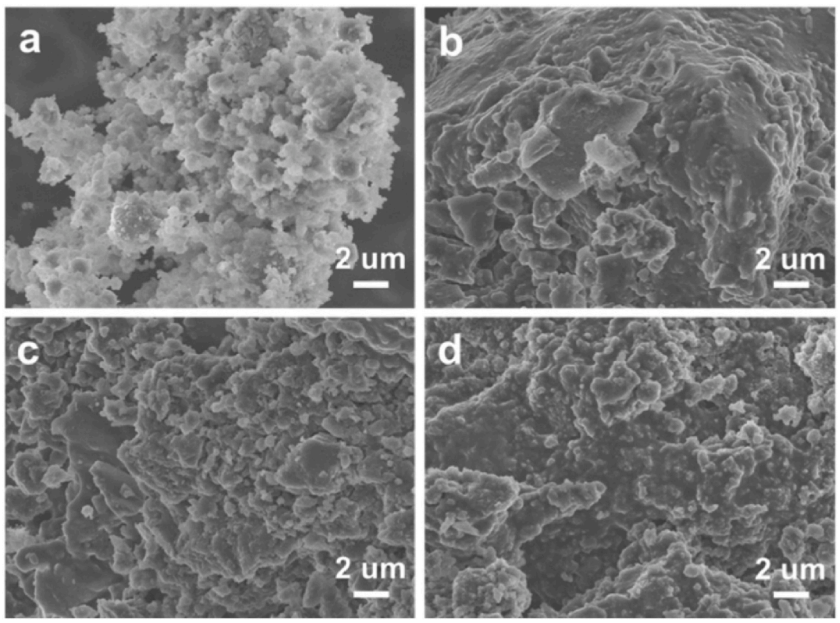

Fig. 4. SEM images of Li_3AlH_6 electrode material at different lithium storage stages. (a) As-prepared Li_3AlH_6, (b) Li_3AlH_6 before discharge (point A), (c) Li_3AlH_6 after full discharge (point E), (d) Li_3AlH_6 after full discharge-recharge (point K).

1 M $LiPF_6$ solution of ethylene carbonate, dimethyl carbonate, and diethyl carbonate. Li_3AlH_6 delivers a reversible capacity of ~676.5 mAh/g at the first cycle. After 100 cycles, it still retains a reversible capacity of 298.7 mAh/g. The irreversible reaction and a large volumetric expansion/contraction in delithiation/lithiation process are the main reasons for the capacity deterioration. As shown in Fig. 3d, the charge capacities of as-prepared Li_3AlH_6 are 456.4, 332.8, and 236.3 mAh/g, respectively, when the current density is 100, 200, and 300 mA/g. However, the current density increased to higher values of 500 and 1000 mA/g, the lithium storage capacities greatly decreased to 121.3 and 57.5 mAh/g, respectively. When the current density returns to 200 mA/g, the capacity still can achieve 341.2 mAh/g. At the 100th cycle, the reversible capacity was 220.4 mAh/g, corresponding to a capacity retention of 55 %. Compared with metal hydroxides anode materials, Li_3AlH_6 shows remarkable lithium storage plateaus in the discharge/charge process whereas the potential plateau is not observed in the discharge/charge curves of metal hydroxides anode materials such as $Ni(OH)_2$ [26,28]. This phenomenon supports that the lithium storage mechanism is different for the lithium aluminum hydride Li_3AlH_6 and metal hydroxides (Table S1).

From the scanning electron microscopy (SEM) images in Fig. 4, the particle size of Li_3AlH_6 electrode material at the different discharge/recharge stages is larger than that of the as-prepared Li_3AlH_6 due to the agglomeration of the fine particles. Fig. 4c and d shows the morphology of Li_3AlH_6 fully discharged and recharged, respectively. The active materials, the LiH and the above-mentioned unknown phases, with small size particle are dispersed on the matrix. The small size particle of LiH can buffer the volume expansion generated in the subsequent lithiation/delithiation process. Therefore, the buffer effect of a matrix and the surface coating of similar SEI layer are considered as the main factor for the improved cycling stability of Li_3AlH_6.

3. Conclusion

In summary, we have reported a complex metal Li_3AlH_6 as anode material toward Li-ion battery, which was prepared by ball milling $LiAlH_4$ and LiH with a molar ratio of 1:2. Li_3AlH_6 electrode material exhibits a discharge capacity of ~1729 mAh/g and a recharge capacity of ~509 mAh/g at the first cycle. Experimental results demonstrated that Li_3AlH_6 can be converted to LiH and LiAl in the first electrochemical lithiation process, however, they are only reverted to LiH and metallic Al in the following delithiation process. Experimental results demonstrate that the electrochemical lithium storage in Li_3AlH_6 is following: $Li_3AlH_6+4Li^++4e^-\rightarrow 6LiH + LiAl\rightarrow 6LiH + Al+Li^++e^-$. In addition, the cycling performance of Li_3AlH_6 is improved via adjusting electrolyte composition. Li_3AlH_6 possesses a high cycling stability due to the buffer effect of a matrix and the surface coating of similar SEI layer. This work demonstrates the significance of developing a novel complex metal toward as anode material toward Li-ion battery.

REAGENT or RESOURCE	SOURCE	IDENTIFIER
Chemicals, peptides, and recombinant proteins		
$LiAlH_4$	Alfa Aesar	CAS Number: 16853-85-3
LiH	Alfa Aesar	CAS Number: 7580-67-8
Other		
Glovebox	MBRAUN	www.mbraun.com
X-ray diffractometer	PANalytical	www.malvernpanalytical.com
Fourier infrared spectrometer	Bruker	Tensor 27
Scanning electron microscopy	Hitachi	S4800
Planetary ball mill	QM-3SP4	WWW.nju-instrument.com
Coin battery tester	Neware	CT-3008W–5V2mA-S4
Electrochemical workstation	Chenhua	Chi660e

4. Resource availability

4.1. Lead contact

Further information and requests for resources and reagents should be directed to and will be fulfilled by the lead contact, Chu Liang(cliang@zjut.edu.cn), Xiaoyu Zhang(zhangxiaoyu@zjut.edu.cn)

4.1.1. Materials availability

This study did not generate new materials.

4.1.2. Data and code availability

- Data reported in this paper will be shared by the lead contact upon request.
- This paper does not report original codes.
- Any additional information required to reanalyze the data reported in this paper is available from the lead contact upon request.

5. Experimental model and subject details

This work did not need any unique experimental model.

6. Method details

6.1. Materials and preparation

$LiAlH_4$ (97 %, Alfa Aesar) and LiH (98 %, Alfa Aesar) were used without further purification. Li_3AlH_6 was synthesized by milling $LiAlH_4$ and LiH with a molar ratio of 1:2 under 1.0 bar argon (Ar) for 24 h on a planetary ball mill (QM-3SP4, Nanjing) rotating at 500 rpm. The ball-to-sample weigh ratio was about 60:1. The electrode materials of Li_3AlH_6 was prepared by milling active materials with acetylene black with weight ratios of 85:15, applied a planetary ball mill with a rotating speed of 350 rpm for 12 h. To prevent contamination from moisture and air, all sample handlings were carried out in a MBRAUN glovebox filled with purified argon (H_2O: $<$1 ppm, O_2: $<$1 ppm).

7. Electrochemical measurements

As-milled electrode material of ~5.0 mg was spread on a nickel foam collector with a diameter of 15 mm. Then, the nickel foam collector was cold pressed under a pressure of 20 MPa. The anode electrode does not contain any binder. Half cells were employed to measure electrochemical properties. A 2025 coin-type cell was assembled by using a Cellgard 2400 microporous membrane as a separator and electrolyte composed of 1 M $LiPF_6$ solution of ethylene carbonate and dimethyl carbonate with a weight ratio of 1:1 or ethylene carbonate, dimethyl carbonate, and diethyl carbonate with a weight ratio of 1:1:1. The fabrication of electrodes and the assembly of coin cells were performed in a MBRAUN glovebox filled with purified argon. The discharge-charge properties were measured on a Neware CT-3008W–5V2mA-S4 Tester (Neware, China) at a temperature of ~25 °C. Cells were discharged from an initial open-circuit potential to 0.005 V *vs* Li^+/Li and cycled between 0.005 V and 3.0 V at a constant current density of 100–1000 mA/g.

8. Quantification and statistical analysis

To obtain the electrode materials at different lithium storage stages, electrochemical measurements were stopped once cells cycled down to a given voltage. The cells were opened and the working electrodes were washed with dimethyl carbonate in a MBRAUN glovebox filled with purified argon. The materials after electrochemical measurements were collected for structural and morphological characterization. Crystal structure of samples was identified by using a X'Pert Pro X-ray diffractometer (PANalytical, The Netherlands) with Cu Kα radiation operated at 40 kV and 40 mA. X-ray diffraction (XRD) data were collected in a 2θ range of 10–90° with a step of 0.05°. During sample transfer and testing, all the samples were maintained under an argon atmosphere using a homemade container. Infrared spectra were measured on a Bruker Tensor 27 Fourier infrared spectrometer (FTIR, Germany). The reflection mode was adopted with a resolution of 4 cm^{-1}. 32 scans were made and accumulated. An *in situ* cell with two KBr windows was used to prevent powder sample from air and moisture contamination in the measurements. A scanning electron microscopy (SEM, Hitachi-S4800) was employed to observe the particle sizes and morphologies of samples at different stages.

CRediT authorship contribution statement

Chu Liang: Funding acquisition, Investigation, Writing – original draft, Writing – review & editing. **Zhangze Ye:** Data curation, Formal analysis, Writing – original draft. **Yaxiong Yang:** Formal analysis. **Huilong Jing:** Data curation. **Haihuang Wu:** Data curation. **Yanxia Liu:** Formal analysis. **Xiaoyu Zhang:** Funding acquisition, Supervision, Writing – review & editing. **Zhihe Liu:** Formal analysis. **Hongge Pan:** Formal analysis, Investigation, Methodology, Supervision.

Declaration of competing interest

The authors declare that they have no known competing financial interests or personal relationships that could have appeared to influence the work reported in this paper.

Acknowledgement

This work was financially supported by the financial supports from the National Key R&D Program of China (2022YFB2502000), the National Natural Science Foundation of China (52072342 and 52001278) and Zhejiang Provincial Natural Science Foundation (Q21E010027).

Appendix A. Supplementary data

Supplementary data to this article can be found online at https://doi.org/10.1016/j.heliyon.2023.e21765.

References

[1] X. Zeng, M. Li, D. Abd El-Hady, W. Alshitari, A.S. Al-Bogami, J. Lu, K. Amine, Commercialization of lithium battery technologies for electric vehicles, Adv. Energy Mater. 9 (2019), 1900161, https://doi.org/10.1002/aenm.201900161.

[2] A. Masias, J. Marcicki, W.A. Paxton, Opportunities and challenges of lithium ion batteries in automotive applications, ACS Energy Lett. 6 (2021) 621–630, https://doi.org/10.1021/acsenergylett.0c02584.

[3] W. Cai, C. Yan, Y.X. Yao, L. Xu, X.R. Chen, J.Q. Huang, Q. Zhang, The boundary of lithium plating in graphite electrode for safe lithium-ion batteries, Angew. Chem. Int. Ed. 60 (2021) 13007–13012, https://doi.org/10.1002/anie.202102593.

[4] L. Zhao, B. Ding, X.Y. Qin, Z. Wang, W. Lv, Y.B. He, Q.H. Yang, F. Kang, Revisiting the roles of natural graphite in ongoing lithium-ion batteries, Adv. Mater. 34 (2022), 2106704, https://doi.org/10.1002/adma.202106704.

[5] L. Jin, C. Shen, Q. Wu, A. Shellikeri, J. Zheng, C. Zhang, J.P. Zheng, Pre-lithiation strategies for next-generation practical lithium-ion batteries, Adv. Sci. 8 (2021), 2005031, https://doi.org/10.1002/advs.202005031.

[6] Y. Han, G. Huang, S. Xu, Structural reorganization-based nanomaterials as anodes for lithium-ion batteries: design, preparation, and performance, Small 16 (2020), 1902841, https://doi.org/10.1002/smll.201902841.

[7] Z. Li, Y. Zhang, T. Liu, X. Gao, S. Li, M. Ling, C. Liang, J. Zheng, Z. Lin, Silicon anode with high initial coulombic efficiency by modulated trifunctional binder for high-areal-capacity lithium-ion batteries, Adv. Energy Mater. 10 (2020), 1903110, https://doi.org/10.1002/aenm.201903110.

[8] H. Tian, H. Tian, W. Yang, F. Zhang, W. Yang, Q. Zhang, Y. Wang, J. Liu, S.R.P. Silva, H. Liu, G. Wang, Stable hollow-structured silicon suboxide-based anodes toward high-performance lithium-ion batteries, Adv. Funct. Mater. 31 (2021), 2101796, https://doi.org/10.1002/adfm.202101796.

[9] Y. Zhang, Z. Mu, J. Lai, Y. Chao, Y. Yang, P. Zhou, Y. Li, W. Yang, Z. Xia, S. Guo, MXene/Si@SiO_x@C layer-by-layer superstructure with autoadjustable function for superior stable lithium storage, ACS Nano 13 (2019) 2167–2175, https://doi.org/10.1021/acsnano.8b08821.

[10] L. Zhang, C. Wang, Y. Dou, N. Cheng, D. Cui, Y. Du, P. Liu, M. Al-Mamun, S. Zhang, H. Zhao, A yolk-shell structured silicon anode with superior conductivity and high tap density for full lithium-ion batteries, Angew. Chem. Int. Ed. 58 (2019) 8824–8828, https://doi.org/10.1002/anie.201903709.

[11] D.C. Zuo, S.C. Song, C.S. An, L.B. Tang, Z.J. He, J.C. Zheng, Synthesis of sandwich-like structured Sn/SnO_x@MXene composite through in-situ growth for highly reversible lithium storage, Nano Energy 62 (2019) 401–409, https://doi.org/10.1016/j.nanoen.2019.05.062.

[12] C. Ke, R. Shao, Y. Zhang, Z. Sun, S. Qi, H. Zhang, M. Li, Z. Chen, Y. Wang, B. Sa, et al., Synergistic engineering of heterointerface and architecture in new-type ZnS/Sn heterostructures in situ encapsulated in nitrogen-doped carbon toward high-efficient lithium-ion storage, Adv. Funct. Mater. 32 (2022), 2205635, https://doi.org/10.1002/adfm.202205635.

[13] Y. Huang, Y. Fang, X.F. Lu, D. Luan, X.W.(D.) Lou, Co_3O_4 hollow nanoparticles embedded in mesoporous walls of carbon nanoboxes for efficient lithium storage, Angew. Chem. Int. Ed. 59 (2020) 19914–19918, https://doi.org/10.1002/anie.202008987.

[14] T. Zhao, R. Ji, Y. Meng, Foamed porous structure Fe-Mn oxides/C composites as novel anode materials of lithium-ion batteries, J. Alloys Compd. 882 (2021), 160643, https://doi.org/10.1016/j.jallcom.2021.160643.

[15] F.X. Ma, H. Hu, H.B. Wu, C.Y. Xu, Z. Xu, L. Zhen, X.W. David Lou, Formation of uniform Fe_3O_4 hollow spheres organized by ultrathin nanosheets and their excellent lithium storage properties, Adv. Mater. 27 (2015) 4097–4101, https://doi.org/10.1002/adma.201501130.

[16] W. Guo, W. Sun, Y. Wang, Multilayer CuO@NiO hollow spheres: microwave-assisted metal-organic-framework derivation and highly reversible structure-matched stepwise lithium storage, ACS Nano 9 (2015) 11462–11471, https://doi.org/10.1021/acsnano.5b05610.

[17] J. Zheng, C. He, X. Li, K. Wang, T. Wang, R. Zhang, B. Tang, Y. Rui, CoS_2–MnS@Carbon nanoparticles derived from metal–organic framework as A promising anode for lithium-ion batteries, J. Alloys Compd. 854 (2021), 157315, https://doi.org/10.1016/j.jallcom.2020.157315.

[18] R. Gao, S. Wang, Z. Xu, H. Li, S. Chen, H. Hou, J. Wang, Octahedral Fe_3O_4/FeS composite synthesized by one-pot hydrothermal method as A high-performance anode material for lithium-ion batteries, J. Alloys Compd. 864 (2021), 158796, https://doi.org/10.1016/j.jallcom.2021.158796.

[19] X. Lin, Z. Yang, A. Guo, D. Liu, Facile synthesis of FeS@C particles toward high-performance anodes for lithium-ion batteries, Nanomaterials 9 (2019) 1467, https://doi.org/10.3390/nano9101467.

[20] X. Zhang, F. Ma, K. Srinivas, B. Yu, X. Chen, B. Wang, X. Wang, D. Liu, Z. Zhang, J. He, Y. Chen, Fe_3N@N-doped graphene as A lithiophilic interlayer for highly stable lithium metal batteries, Energy Stor. Mater. 45 (2022) 656–666, https://doi.org/10.1016/j.ensm.2021.12.010.

[21] H. Huang, S. Gao, A.M. Wu, K. Cheng, X.N. Li, X.X. Gao, J.J. Zhao, X.L. Dong, G.Z. Cao, Fe_3N constrained inside C nanocages as an anode for Li-ion batteries through post-synthesis nitridation, Nano Energy 31 (2017) 74–83, https://doi.org/10.1016/j.nanoen.2016.10.059.

[22] M. Ashuri, Q. He, L.L. Shaw, Silicon as A Potential anode material for Li-ion batteries: where size, geometry and structure matter, Nanoscale 8 (2016) 74–103, https://doi.org/10.1039/c5nr05116a.

[23] M. Ge, C. Cao, G.M. Biesold, C.D. Sewell, S.M. Hao, J. Huang, W. Zhang, Y. Lai, Z. Lin, Recent advances in silicon-based electrodes: from fundamental research toward practical applications, Adv. Mater. 33 (2021), 2004577, https://doi.org/10.1002/adma.202004577.

[24] J. Wu, P. Zhang, X. Chen, Y. Wang, Q. Zhang, S. Yu, M. Wu, Erythrocyte-like single crystal α-Fe_2O_3 anode synthesized by facile one-step hydrothermal method for lithium-ion battery, Chemelectrochem 9 (2022) 1702–1707, https://doi.org/10.1002/celc.202200863.

[25] S. Zhong, S. Ju, Y. Shao, W. Chen, T. Zhang, Y. Huang, H. Zhang, G. Xia, X. Yu, Magnesium hydride nanoparticles anchored on MXene sheets as high capacity anode for lithium-ion batteries, J. Energy Chem. 62 (2021) 431–439, https://doi.org/10.1016/j.jechem.2021.03.049.

[26] J.H. Yao, R.S. Huang, Y.W. Li, K. Luo, B. Huang, Facile hydrothermal fabrication of an α-$Ni(OH)_2$/N-doped reduced graphene oxide nanohybrid as A high-performance anode material for lithium-ion batteries, Energy Fuels 37 (2023) 2368–2378, https://doi.org/10.1021/acs.energyfuels.2c03341.

[27] P. Gao, S. Ju, Z. Liu, G. Xia, D. Sun, X. Yu, Metal hydrides with in situ built electron/ion dual-conductive framework for stable all-solid-state Li-ion batteries, ACS Nano 16 (2022) 8040–8050, https://doi.org/10.1021/acsnano.2c01038.

[28] K. Luo, Y.W. Li, J.H. Yao, B. Huang, Q. Zhu, J. Yang, Boosting the lithium storage property of nickel-zinc layered double hydroxides by intercalation with dodecyl sulfate anions, Appl. Surf. Sci. 620 (2023), 156850, https://doi.org/10.1016/j.apsusc.2023.156850.

[29] S. Kim, H. Oguchi, N. Toyama, T. Sato, S. Takagi, T. Otomo, D. Arunkumar, N. Kuwata, J. Kawamura, S.I. Orimo, A complex hydride lithium superionic conductor for high-energy-density all-solid-state lithium metal batteries, Nat. Commun. 10 (2019) 1081, https://doi.org/10.1038/s41467-019-09061-9.

[30] J.B. Grinderslev, L.N. Skov, J.G. Andreasen, S. Ghorwal, J. Skibsted, T.R. Jensen, Methylamine lithium borohydride as electrolyte for all-solid-state batteries, Angew. Chem. Int. Ed. 61 (2022), 202203484, https://doi.org/10.1002/anie.202203484.

[31] F. Mo, X. Chi, S. Yang, F. Wu, Y. Song, D. Sun, Y. Yao, F. Fang, Stable three-dimensional metal hydride anodes for solid-state lithium storage, Energy Stor. Mater. 18 (2019) 423–428, https://doi.org/10.1016/j.ensm.2019.01.014.

[32] P. Black, The structure of $FeAl_3$. I, Acta Crystallogr. 8 (1955) 43–48, https://doi.org/10.1107/S0365110X5500011X.

[33] F. Thoss, L. Giebeler, S. Oswald, H. Ehrenberg, J. Eckert, Study on the reversible Li-insertion of amorphous and partially crystalline $Al_{86}Ni_8La_6$ and $Al_{86}Ni_8Y_6$ alloys as anode materials for Li-ion batteries, Electrochim. Acta 60 (2012) 85–94,, https://doi.org/10.1016/j.electacta.2011.11.016.